A time-series analysis of blood-based biomarkers within a 25-year longitudinal dolphin cohort.

Aaditya V. Rangan[1*], Caroline C. McGrouther[1], Nivedita Bhadra[2], Nicholas J. Schork[2],

1 Courant Institute of Mathematical Sciences, New York University, New York, NY, United States of America
2 The Translational Genomics Research Institute, Quantitative Medicine and Systems Biology, Phoenix, AZ, United States of America

* avr209@nyu.edu

1 Abstract

Causal interactions and correlations between clinically-relevant biomarkers are important to understand, both for informing potential medical interventions as well as predicting the likely health trajectory of any individual as they age. These interactions and correlations can be hard to establish in humans, due to the difficulties of routine sampling and controlling for individual differences (e.g., diet, socio-economic status, medication). Because bottlenose dolphins are long-lived mammals that exhibit several age-related phenomena similar to humans, we analyzed data from a well controlled 25-year longitudinal cohort of 144 dolphins. The data from this study has been reported on earlier, and consists of 44 clinically relevant biomarkers. This time-series data exhibits three starkly different sources of variation: (A) deterministic interactions between biomarkers, (B) stochastic drive that can either correlate or decorrelate different biomarkers, and (C) an observation noise which combines measurement error and very rapid fluctuations in the dolphin's biomarkers. Importantly, the stochastically-driven correlations (type-B) are large in magnitude, often comparable to the obervation errors (type-C) and larger than the deterministic interactions (type-A). Attempting to recover the type-A interactions without accounting for the type-B and type-C variation can result in an abundance of false-positives and false-negatives. Using a generalized regression which fits the longitudinal data with a linear model accounting for all three sources of variation, we demonstrate that the dolphins exhibit several significant deterministic interactions (type-A), as well as many significant stochastically-driven correlations (type-B), between several pairs of biomarkers. Moreover, many of these interactions are associated with advanced age, suggesting that these interactions can be monitored and/or targeted to predict and potentially affect aging.

2 Introduction

A better understanding of the biology of aging can help us discover strategies to stay healthier longer [1, 2]. Studying aging directly in humans has many advantages, and can help pinpoint some of the mechanisms responsible for predicting and controlling aging rates [3, 4, 5, 6, 7]. Unfortunately, human studies have several disadvantages, including difficulties acquiring regular samples, as well as controlling for the variations between individuals (e.g., diet, socioeconomic status and medication) [6, 8, 9]. Many of these limitations can be overcome by focusing on short-lived animals such as worms, flies and mice [10, 11], but it is important to complement this work with studies of animals that have lifespans similar to humans (i.e., with evolutionary adaptations that allow them to live 50 or more years long).

Bottlenose dolphins (*Tursiops truncatus*) provide a useful model organism, as they are long-lived mammals which perform complex social and cognitive tasks over the course of their lives [12, 13, 14, 15]. Importantly, dolphins also share many genetic and biogerontological qualities with humans [16, 14, 17, 18, 19, 20, 21, 22]. For example, dolphins exhibit some similarities to humans regarding cellular function [23], and reduce their energy expenditure as they age [24]. Dolphins also develop several age-related conditions – such as chronic inflammation and insulin-resistance – with clinical signs similar to humans [18, 22, 25, 26, 27], while also developing histological lesions similar to certain human disorders [26, 27, 28, 29, 30].

In this manuscript we analyze data taken from a longitudinal cohort of 136 US Navy bottlenose-dolphins. These dolphins were cared for over three generations and were routinely sampled to asess the trajectory of 44 clinically relevant biomarkers over their lifespan, as described in [20, 31, 32]. The diet and environment of these dolphins was carefully controlled, resulting in the dolphins living an average of 32.5 years (c.f. wild dolphins live an average of 20 years) [33, 34]. The uniformity of environment, diet and health-care within this this cohort implies that age-related differences between dolphins might be due to inherent or genetic factors influencing senescence [35].

This data-set was used previously to demonstrate differences in aging-rates between individual dolphins [35]. Motivated by these results, we further analyze the trajectories of each of the biomarkers for each of the dolphins within this data-set, searching for hints of any causal interactions between the measured biomarkers. In this analysis it is crucial to account for the shared variation between variables, as this shared variation typically dwarfs the more subtle deterministic interactions

we are trying to find. To account for this shared variation, we model the longitudinal data as a linear stochastic-differential-equation (SDE), extracting model parameters as indicators of which variables might affect one another. After doing so, we are able to identify interactions that are associated with aging. These interactions may play a role in the biology of aging, and are prime candidates for further investigation.

3 Results

3.1 Motivation for the Model

Obviously, the body is a very complicated dynamical system [36]. Any set of biomarkers can only ever tell part of the story, and there will always be an abundance of unmeasured factors that play an important role in the trajectory of all the measured biomarkers. Thus, given any particular subset of (observed) biomarkers, there will typically be some deterministic interactions between those variables, but also a source of variation coming from unobserved variables. We will refer to the former as 'type-A' interactions, and the latter as 'type-B'.

Regarding the former, we'll model the type-A interactions as simple linear interactions (see (1) below). For the latter, we expect the type-B influence of unmeasured variables to look like a kind of shared noise influencing the measured variables. As illustrated in Fig 1, the distribution of increments for the 'Alkaline Phosphate' (AlkPhos) variable indicates that a significant component of the type-B variation appears similar to the stochastic drive commonly seen in high-dimensional dynamical systems [37]. This shared stochastic drive manifests as an (anisotropic) gaussian-process with time-dependent variance [38]. Notably, the variance scales roughly linearly with the magnitude of the time-increment, as would be the case if this variance were driven by a Brownian-process. Figures 2 and 3 illustrate the distribution of increments for two other variables. Motivated by this observation, we'll model the type-B variation as an (anisotropic) Brownian-process (see (1) below).

As one can clearly see in Figs 1-3, the variables typically exhibit variation even when the time-increment between measurements is small (or even 0). In other words, multiple repeated measurements of the same dolphin may not always return the same value. We'll refer to this source of variation as 'type-C' variation.

This type-C variation can include both measurement errors as well as true biological fluctuations that are much more rapid than the typical time-interval of the experimental measurements themselves (e.g,. hourly variations based on the individual's activity). We will model this observation-noise as an (anisotropic) gaussian with time-independent variance [38] (see (2) below)..

For some variables we expect the type-B variation to be larger than the type-C variation, whereas for other variables we expect the type-C variation to dominate (e.g., compare Figs 2 and 3).

3.2 Model Structure

Given the motivation above, we can model the evolution of any d specific variables over the time-interval $[t, t']$ using a simple linear stochastic-differential-equation (SDE) of the following form:

$$dX(t) = [\boldsymbol{a} + A \cdot X(t)]\, dt + B \cdot dW(t), \tag{1}$$

where $X(t) \in \mathbb{R}^d$ represents the d-dimensional vector-valued solution-trajectory at the initial time t, the time-increment $dt = t' - t$ represents the difference between the initial time t and the final time t', and $dX(t) = X(t') - X(t) \in \mathbb{R}^d$ represents the vector of variable-increments between times t and t'. The vector $\boldsymbol{a} \in \mathbb{R}^d$ accommodates a constant drift for each of the variables, and the matrix $A \in \mathbb{R}^{d\times d}$ represents the deterministic type-A (linear) interactions between variables. The type-B variation is modeled by the brownian-increments $dW(t)$, each drawn independently from the gaussian distribution $\mathcal{N}(0, dt \cdot I_{d\times d})$. The matrix $B \in \mathbb{R}^{d\times d}$ controls the anisotropy of the type-B variation; the covariance of this stochastic term is given by the symmetric-matrix $dtBB^{\intercal}$ [37]. We assume that we do not measure $X(t)$ directly, but rather some $Y(t)$ which depends on $X(t)$, but which also incorporates the type-C observation-noise:

$$Y(t) = X(t) + C \cdot \boldsymbol{\epsilon}(t), \tag{2}$$

where each vector $\boldsymbol{\epsilon}(t) \in \mathbb{R}^d$ at each observation-time is drawn (independently) from the gaussian distribution $\mathcal{N}(0, I_{d\times d})$. The matrix $C \in \mathbb{R}^{d\times d}$ controls the anisotropy of the type-C errors; the covariance of this observation-error is given by the symmetric-matrix $CC^{\intercal}$.

Note that the observation-times are not necessarily unique: t' could very well equal t, and dt may equal 0. In this situation $dX(t) \equiv \mathbf{0}$, and so $X(t')$ will equal $X(t)$. However, because of the type-C errors, $Y(t')$ will in general be different from $Y(t)$.

While we could, in principle, fit an SDE to all the variables simultaneously (with a large d), we opt to consider only pairwise combinations of variables (with $d = 2$ in each case). Mathematically, each such pairwise fit (for variables v and v') corresponds to approximating the system's trajectory after projecting the full system onto the subspace spanned by those two variables. We make this decision for three reasons.

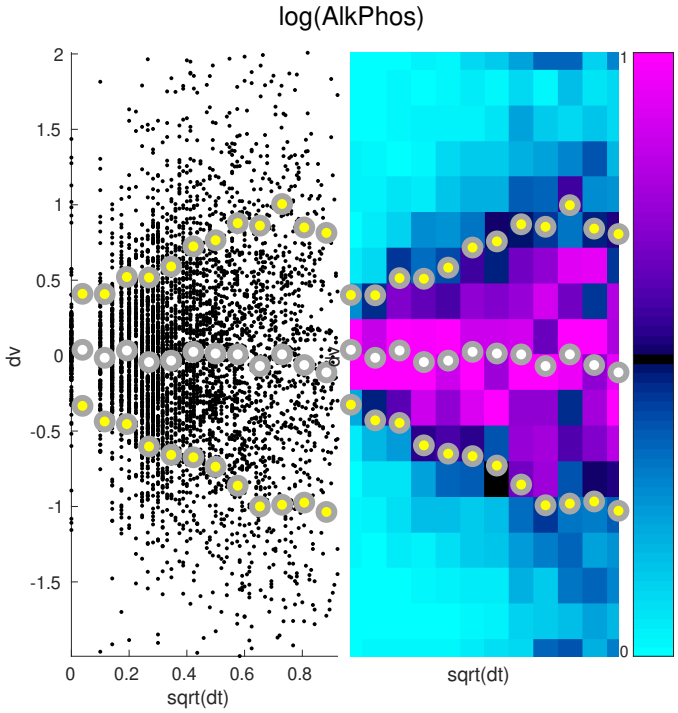

Figure 1: Here we illustrate the distribution of increments associated with Alkaline Phosphate (AlkPhos). On the left we show a scatterplot of these increments. Each small black point in the background represents a pair of time-adjacent measurements in a single dolphin, with the square-root of the time-increment (in years) along the horizontal, and the change in AlkPhos along the vertical. The time-increments are then divided into 12 bins, and the mean (white dot) plus and minus one standard-deviation (yellow dots) are displayed in the foreground. On the right we show the same data, with the 12 time-bins shown as vertical strips. Each vertical strip is further divided into 18 boxes, which are colored by the number of increments within that time-bin which fall into that box (i.e., a histogram for each time-bin, scaled to have maximum 1, colored as shown in the colorbar to the far right). Note that the distribution of increments for each time-bin becomes wider as the time-increment increases. Importantly, the standard-deviation increases roughly linearly with the square-root of the time-increment (i.e., the variance increases roughly linearly with the time-increment), as expected from a Brownian-process. Note also that the variance is nonzero even when the time-increment is 0, implying that there must be an extra source of variation in addition to this Brownian-process.

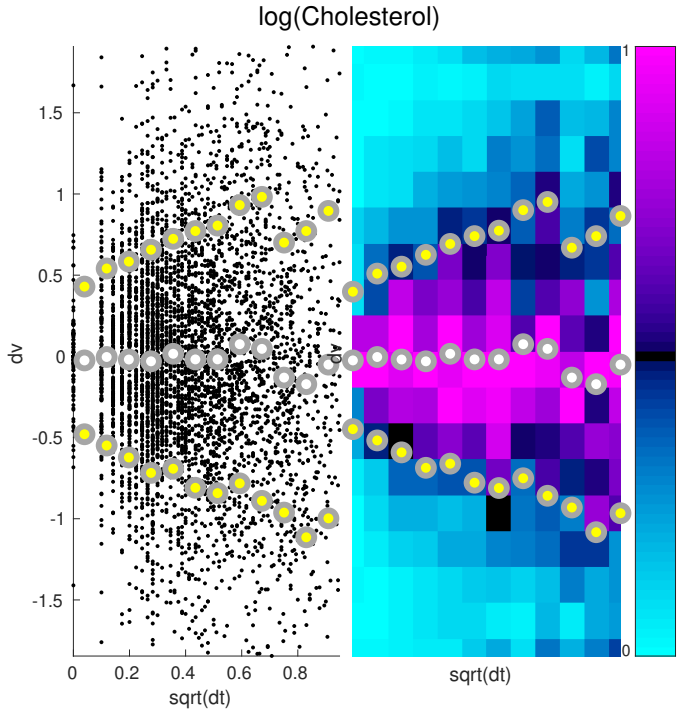

Figure 2: Here we illustrate the distribution of increments associated with Cholesterol. The format for this figure is the same as Fig 1.

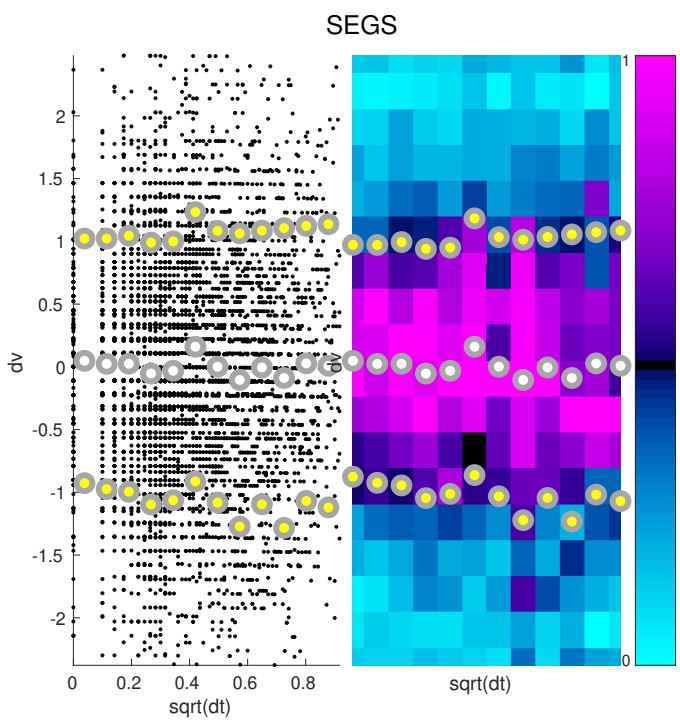

Figure 3: Here we illustrate the distribution of increments associated with Segmented Neutrophils (SEGS). The format for this figure is the same as Fig 1.

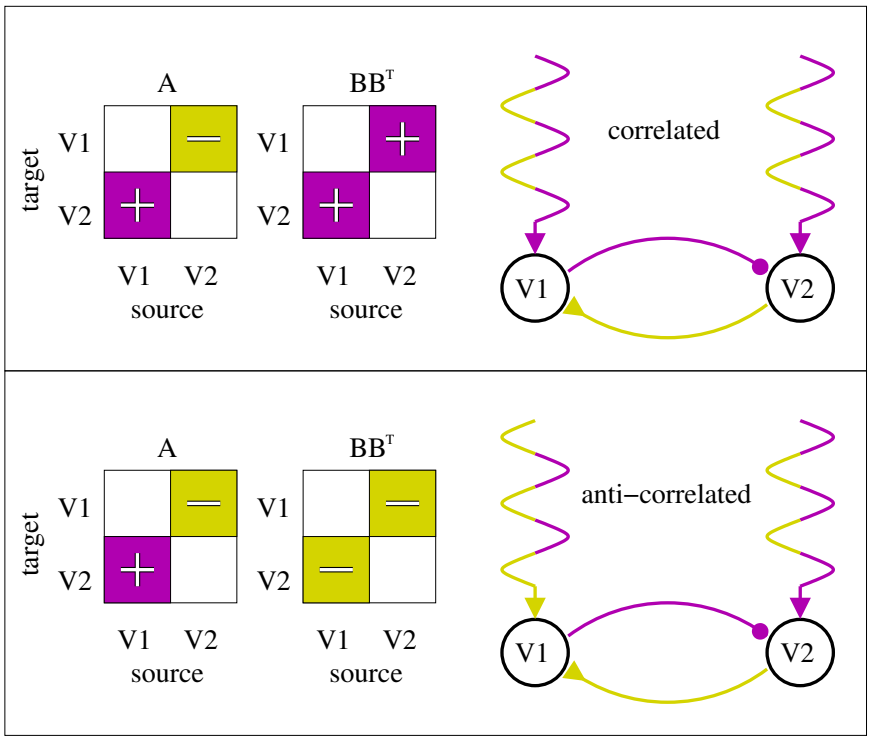

Figure 4: Here we illustrate the different kinds of interactions modeled by the SDE. The matrix-entries $A_{vv'}$ represent deterministic interactions between variables v' and v. If $A_{vv'}$ is positive (or negative), we expect variable v' to have an excitatory (resp. inhibitory) effect on variable v. The matrix-entries $[BB^{\intercal}]_{vv'}$ represent the (shared) stochastic drive to the two variables v and v'. We expect this stochastic drive to come from the accumulated influence of other 'hidden' (or potentially unmeasured) variables. If $[BB^{\intercal}]_{vv'}$ is positive (or negative) we expect the stochastic drive to be correlated (or anti-correlated) across v and v'.

Increase Power: First and foremost, the number of model parameters, as well as the number of observations required to accurately estimate these parameters, both increase as d increases. We will have the most statistical power when d is low.

Avoid Redundancy: Second, redundancies in any subset of variables (e.g., GFR and Creatinine, or MCH and MCV) can easily create the illusion of large interactions between the redundant set and other variables. These spurious interactions will be statistically, but not biologically significant. In mathematical terms, these redundancies will result in a poorly conditioned inverse problem, which we want to avoid [39].

Easily Understand: By considering only pairwise interactions, the results can be interpreted more easily. The interactions between any pair of variables can then be considered (and used to make predictions) even in situations where the other variables aren't accessible, or haven't been measured.

We acknowledge that there are many strategies for modeling the interactions in this longitudinal data-set (see, e.g., [40, 41, 42]). For example, there are many similarities between our model and vector-autogregression [43]. Indeed, if the time-intervals dt in this data-set were all of equal size, then our method would be equivalent to one-step vector-autogregression; the only structural difference being that in such a scenario the type-B and type-C variation would be indistinguishable from one another. We opt for the SDE proposed above because (i) it has relatively few parameters, (ii) it is easy to understand, and (iii) it can easily accommodate the irregular time-intervals and occasional missing elements within this data-set.

3.3 Model Interpretation

We use a generalized regression (see methods) to fit the longitudinal data for each pair of variables v and v' with the simple dynamical system (SDE) above. After fitting the model parameters we interpret A and $BB^{\intercal}$ as having potential biological significance. An illustration of this interpretation is shown in Fig 4

The entries $A_{vv'}$ indicate the deterministic effect on variable v from variable v'. If $A_{vv'}$ is positive, then we expect an increase in variable v' to typically precede a subsequent increase in variable v; we conclude that v' 'excites' v. Conversely,

if $A_{vv'}$ is negative, then we expect that v' will 'inhibit' v; an increase in v' will typically precede a subsequent decrease in v.

The symmetric entries $[BB^\intercal]_{vv'} = [BB^\intercal]_{v'v}$ indicate the kinds of correlations expected from the shared stochastic drive to the variables v,v'. If $[BB^\intercal]_{vv'}$ is positive, then v and v' will experience correlated stochastic input which will give rise to correlated (but not causal) fluctuations between these two variables. Conversely, if $[BB^\intercal]_{vv'}$ is negative, then v and v' will experience anti-correlated stochastic input which will produce anti-correlated (but again, not causally-linked) fluctuations between the two variables. Because we fit the SDE to each pair of variables individually, the correlations (or anti-correlations) within this stochastic drive to the pair v, v' can result from the accumulated effects of the other measured variables (other than v, v'), as well as from variables which weren't included in the study at all.

To illustrate these kinds of relationships, we fit the SDE in (1),(2) to the two variables 'Iron' and 'Mean corpuscular hemoglobin' (MCH) across all observation-times across all dolphins. Referring to Iron and MCH as v' and v, respectively, we find that $A_{vv'}$ is significantly positive and $A_{v'v}$ is significantly negative (with uncorrected p-values $p_0 < 1\text{e}-11$ and $p_0 < 1\text{e}-4$ respectively, see Methods). Moroever, we find that $[BB^\intercal]_{vv'}$ is significantly positive ($p_0 < 1\text{e}-50$). As we'll discuss below, the type-B correlations are quite a bit larger (in magnitude) than the type-A interactions for these two variables (note the difference in p-values), and an accurate estimate of $A_{vv'}$ can only be obtained after accurately estimating $[BB^\intercal]_{vv'}$.

The deterministic interactions A can be visualized using the phase-diagram of the linear differential-equation associated with A (i.e., by ignoring the effect of B in (1)). This phase-diagram is shown on the left of Fig 5, with the deterministic interactions giving rise to the flow vectors in the background (grey). For this differential-equation a surplus of Iron will drive an increase in MCH, while a surplus of MCH will drive a decrease in Iron. This combination of excitation and inhibition will tend to give rise to 'counterclockwise' motion within the Iron-MCH phase-plane (indicated by the directions of the grey arrowheads).

The subplot on the left of Fig 5 also shows a sample trajectory $X(t)$ of the SDE (which includes the effect of the nonzero B). This trajectory is colored by age, from 0yr (cyan) to 55yr (magenta) (see adjacent colorbar). Note that the sample-trajectory often deviates from the counterclockwise course suggested by the deterministic interactions, often meandering around due to the stochastic drive provided by B. Subplots illustrating the (kalman filtered) trajectories of several individual dolphins are shown on the right of this figure, using the same colorscale. Similar to the sample trajectory from the SDE, these experimental trajectories also meander around, while exhibiting a global tendency to prefer counterclockwise loops over clockwise ones.

The type-B and type-C variations in these two variables are shown in Fig 6. To illustrate these sources of variation, we take all the time-increments dt used to fit the SDE (across all pairs of adjacent observation-times and all dolphins), and divide them into 10 percentile-bands. For each percentile-band of dt we construct a scatterplot of the observed variable-increments $dY(t) \in \mathbb{R}^2$ for these two variables. We fit the distribution of variable-increments in each percentile-band with a gaussian, and indicate the 1- and 2-standard-deviation contours of this gaussian with bright- and pale-yellow ellipses, respectively. The covariance-matrix $CC^\intercal$ is approximately equal to the covariance of the scatterplot shown in the upper-left, with $dt \sim 0$. The covariance-matrix for each of the other subplots is roughly given by $dtBB^\intercal + CC^\intercal$; as dt increases the variable-increments become more and more correlated, indicating that $[BB^\intercal]_{vv'}$ is positive (i.e., these two variables are influenced by a shared and correlated stochastic drive).

For these two variables the type-B and type-C variations contribute heavily, dominating the evolution of the trajectory of the SDE. Specifically, the term $B \cdot dW(t)$ in (1) contributes roughly 6 times as much as the term $A \cdot X(t)dt$ does (on average) to the typical increments observed. The term $C \cdot \boldsymbol{\epsilon}$ in (2) is not small either, giving rise to a contribution that is roughly 2 times as much (on average) as that of the type-A interactions. This is quite common, and most variable-pairs exhibit a similar phenomenon.

If we were to ignore the type-B and/or type-C interactions when fitting this data (i.e., setting $B \equiv 0$ in (1) or $C \equiv 0$ in (2)), then the correlations in these variations would impact our recovery of A, giving rise to inaccurate estimates of $A_{vv'}$. These spurious estimates for $A_{vv'}$ would, in turn, give rise to an abundance of false-positives and false-negatives when estimating the significance of the deterministic interactions across the variable-pairs within the data-set. By accounting for these type-B and type-C terms within the SDE, we believe that we can accurately estimate the size and direction of the deterministic type-A interactions.

To summarize, we expect Iron and MCH to exhibit strong correlated (but not necessarily causal) fluctuations due to shared input coming from the accumulated effect of other (potentially unmeasured) variables. By taking into account these strong type-B correlations, we can attempt to tease out more subtle deterministic type-A interactions. For these two variables we do indeed find evidence of a statistically significant deterministic link: an increase in Iron will tend to produce a subsequent increase in MCH, while an increase in MCH will tend to produce a subsequent reduction in Iron.

3.4 Longitudinal Analysis

By fitting the longitudinal data with the SDE (1),(2) above, we observe multiple significant (type-A) deterministic interactions, as well as (type-B) stochastically-driven correlations. An illustration of the type-A interactions observed across

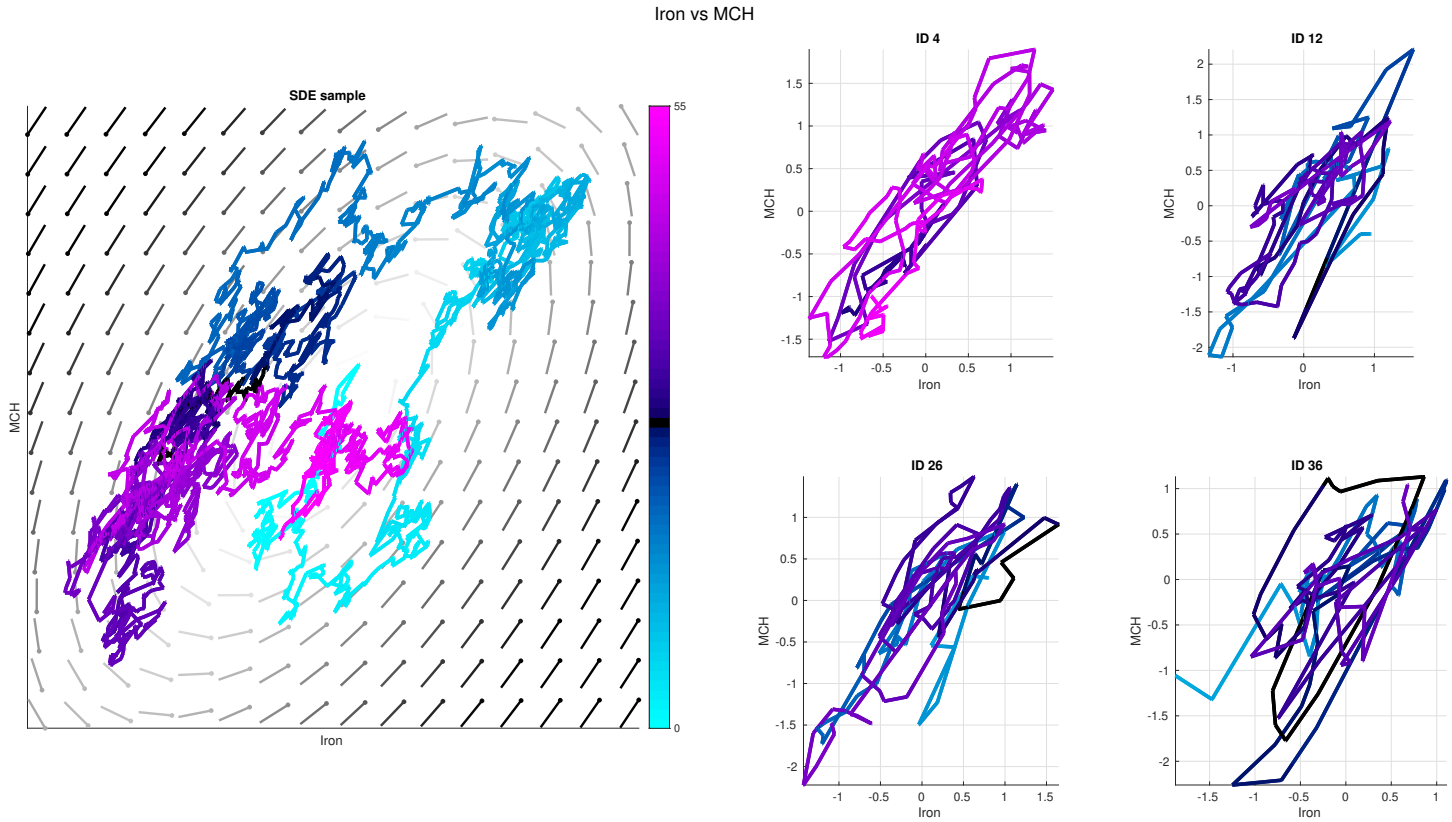

Figure 5: Here we illustrate the deterministic interactions between Iron (horizontal) and mean corpuscular hemoglobin (MCH) (vertical). The left-hand-side shows the phase-diagram associated with A, as well as a sample-trajectory from the SDE (including B). The right-hand-side shows several subplots from various dolphins (after kalman filtering to reduce the observation error). The colorscale refers to age (see inset colorbar).

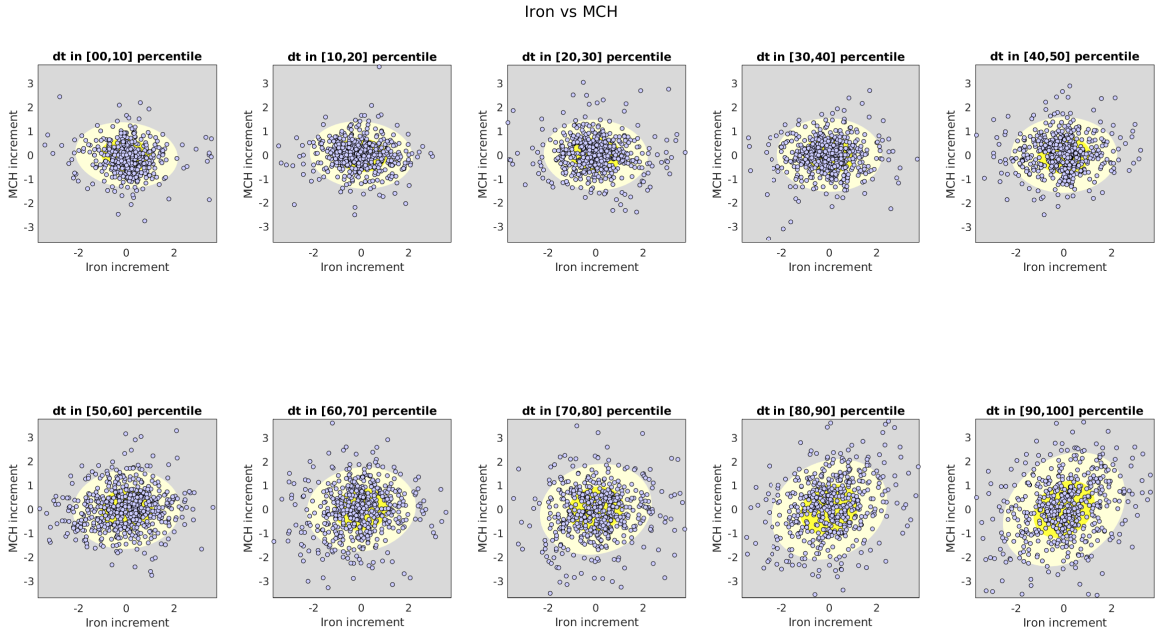

Figure 6: Here we illustrate the type-B and type-C variations associated with Iron (horizontal) and MCH (vertical). Each subplot shows a scatterplot of variable-increments for a percentile-band of observed time-increments. The yellow ellipses correspond to standard-deviation contours of the best-fit gaussian distribution within each scatterplot.

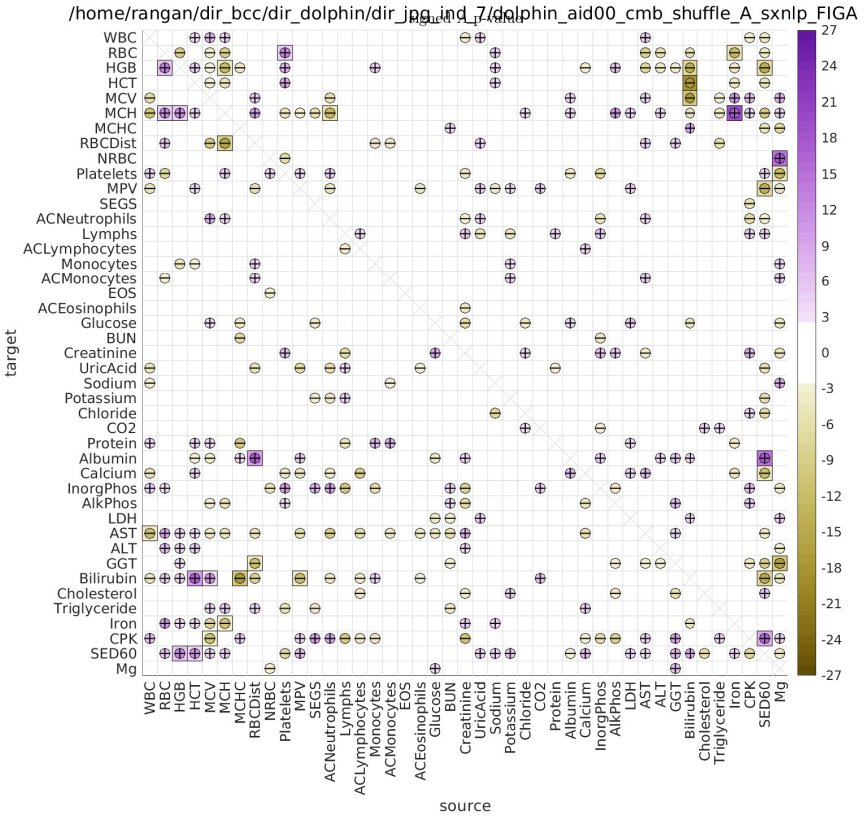

Figure 7: Here we illustrate the significant deterministic interactions $A_{vv'}$ observed when pooling all dolphins and all ages. The 'source' variable v' is shown along the horizontal, with the 'target' v shown along the vertical. The color of each interaction indicates the log-p-value for that interaction, ascribed a sign according to the sign of the interaction. Thus, interactions are colored lavender if the interaction is positive, and goldenrod if the interaction is negative (see colorbar on the right). For ease of interpretation, interactions are also given a '+' or '-' symbol to indicate their sign. The bonferroni-corrected p-values p_b are shown as squares, while the inscribed circles indicate the associated holm-bonferroni adjusted p_h.

all dolphins and ages is shown in Fig 7, while the corresponding type-B correlations are shown in Fig 8.

We first remark that the type-B correlations typically dominate the type-A interactions. We saw an example of this earlier when considering the case of Iron versus MCH, and the same general trend holds for most of the variable pairs. Many strong type-B correlations can be observed between the variables relating to red blood cells (RBCs) and hemoglobin (HGB), such as Iron, RBC, HGB, HCT, MCV, MCH and MCHC. These correlations are to be expected, because many of these variables are influenced by the same underlying biological factors [44, 45]. Similarly, we see many strong type-B correlations between the variables relating to liver function, such as LDH, AST, ALT and GGT. Once again, these are all influenced by the same factors, and strong correlations are to be expected [46, 47].

Regarding the type-A interactions, we note that most of the more significant type-A interactions involve an $A_{vv'}$ and $A_{v'v}$ with opposite signs. That is, one variable excites the other, while being inhibited in return (see, e.g., the interaction between Iron and MCH mentioned earlier). These 'push-pull' pairs manifest when the observed data for variables v and v' both look like noisy versions of the same rough trajectory (e.g., meandering back-and-forth), but with one of the variables 'leading' the other in time. The linear SDE that best fits this scenario is usually one which gives rise to stochastic oscillations with a distribution of temporal correlations fit to what was observed in the real data.

Some of the more statistically significant push-pull interactions include: (i) Iron $\rightleftharpoons$ MCH, (ii) HGB $\rightleftharpoons$ SED60, (iii) HCT+MCH $\rightleftharpoons$ Bilirubin, and (iv) HGB $\rightleftharpoons$ MCH. These interactions suggest an intricate interplay between Iron, various RBC attributes, and inflammation (for which SED60 is a proxy). These interactions are not without precedent in humans. For example, inflammation is well known to have wide-ranging effects, and can alter red blood cell clearance as well as red blood cell counts [48, 49]. The production and regulation of Heme and Hemoglobin also involves many mechanisms, and can be affected by inflammation, in turn affecting endothelial cell activation [50, 51, 52, 53, 54]. The breakdown and/or destruction of RBCs can also release damage-associated molecular patterns which can activate inflammatory pathways [55], and result in increased bilirubin levels, which in turn can trigger erythrocyte death [56].

To search for age-associated interactions, we checked if there were significant differences between the older dolphins

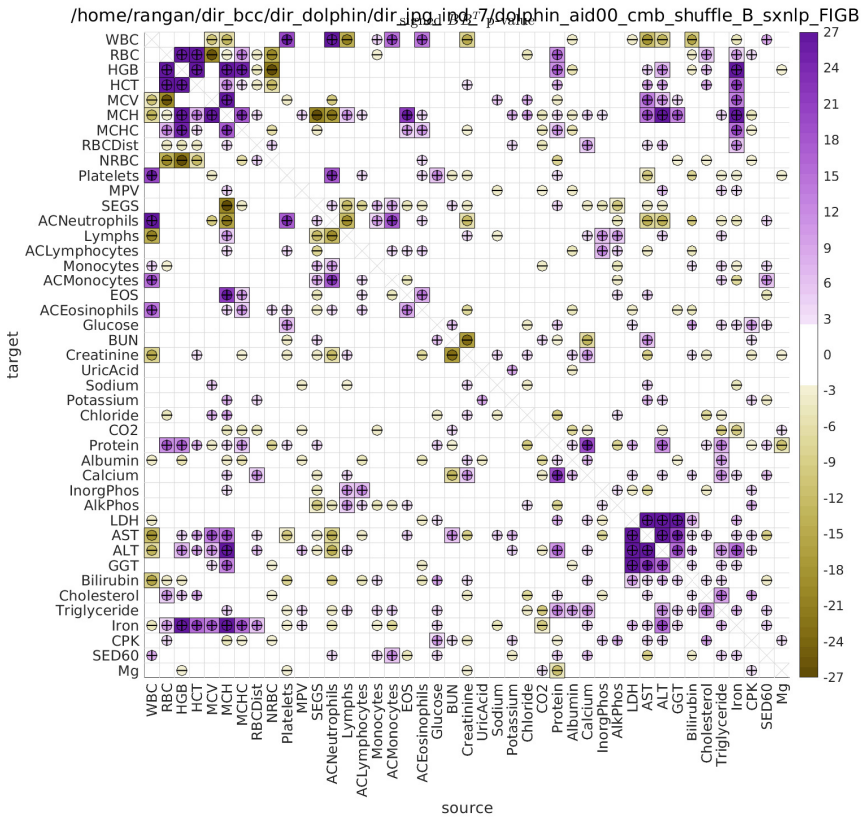

Figure 8: This figure has the same format as Fig 7, showing the stochastic correlations $[BB^{\intercal}]_{vv'}$. As in Fig 7, these results refer to pooling all dolphins and all ages.

(older than 30) and the middle-aged dolphins (between 10 and 30 years old). The results for the type-A interactions are shown in Fig 9 (with the type-B correlations shown in the Supplementary Material). While we saw very few significant differences in the deterministic interactions between the male- and female-dolphins overall in this data-set (the only exceptions being the influence of magnesium on platelets and inorganic phosphate), several previous studies have found significant differences between the sexes [33, 57, 26, 34]. Consequently, we repeated our analysis after segregating by sex. These results are shown in Figs 10 and 11.

While our sex-segregated analysis has lower power than when the sexes were pooled, we can already see that many of the significant differences observed in the general population are in fact driven by one sex or the other. For example, the male dolphin population drives the age-related change in the push-pull deterministic interaction between RDW and MCV. On the other hand, the female dolphin population drives many of the other observed age-related changes, such as the interaction between MCHC and RDW, and the interaction between Magnesium and Glucose.

The age-related changes we observe between RDW and MCV could reflect a change in the regulation of bone-marrow function, or the onset of certain kinds of iron-deficiency anemias [58, 59, 60, 61]. More generally, RDW plays a role in various cardiovascular diseases, and it is possible that RDW serves as a proxy for the body's ability (or lack thereof) to tightly regulate certain processes [62, 63, 64]. Moreover, the management of RDW seems to be important for aging, with at least one study reporting a larger effect-size in men [65, 66].

Regarding the observed interaction between Magnesium and glucose, magnesium is known to affect blood glucose levels and glucose metabolism in humans, and was found to influence glucose absorption in rats [67, 68, 69]. Moreover, magnesium can play the role of a secondary messenger for insulin action, and magnesium accumulation is in turn influenced by insulin [70, 71]. Aging is also associated with changes in magnesium level, and magnesium deficits may result from many age-related conditions [72]. As just one example, the modulation of magnesium levels in elderly patients can potentially improve both insulin response and action, affecting blood glucose levels in turn [73].

4 Conclusions

We have used a linear SDE to model the time-series data from a longitudinal cohort of dolphins. Importantly, this model accounts for stochastic correlations between variables, without which we would not have been able to accurately estimate

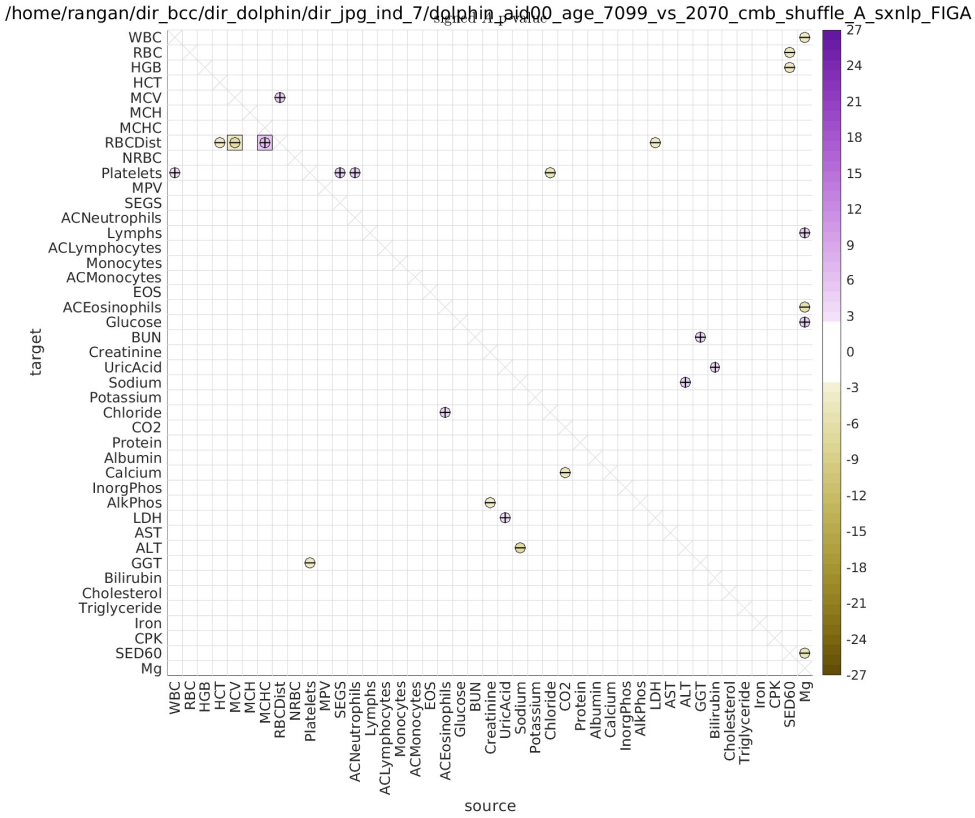

Figure 9: This figure illustrates the significant differences in the deterministic interactions $A_{vv'}$ between (i) dolphins over age 30 and (ii) dolphins between the ages of 10 and 30. Positive signs indicate that the corresponding interaction is more positive in the first group (i.e., dolphins over 30) than in the second group (i.e., dolphins between 10 and 30). Negative signs indicate the reverse.

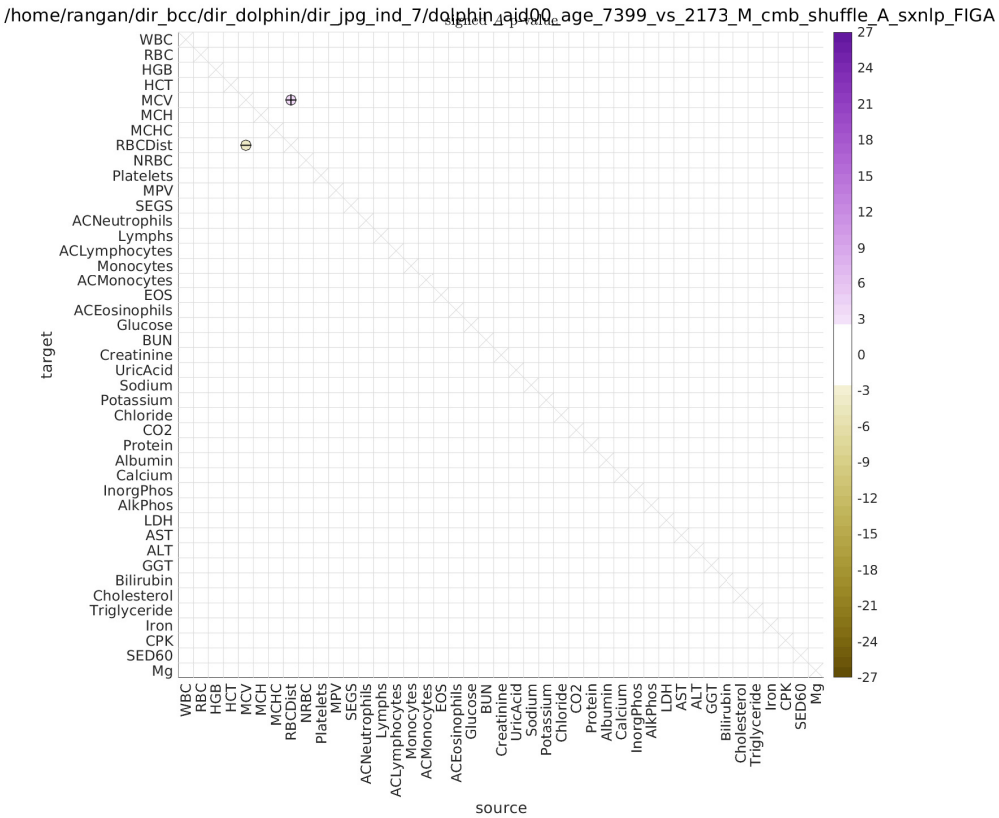

Figure 10: Here we illustrate significant differences in the deterministic interactions $A_{vv'}$ between (i) male dolphins over age 30 and (ii) male dolphins between the ages of 10 and 30.

the deterministic interactions. After performing our analysis, we observed many statistically significant interactions across the population as a whole. We also reported several significant age-related changes to the interaction patterns. Some of the most significant age-related effects involve RDW, MCV and MCHC (in males and females), and the connection between magnesium and glucose (in females).

While certainly suggestive, our a-posteriori analysis cannot be used to decide whether these deterministic interactions are truly causal or not. Indeed, any significant type-A relationship between any pair of variables (such as Iron and MCH shown in Fig 5) might be due to an unmeasured source affecting both variables, but with different latencies. In this scenario both variables would receive the same unmeasured signal, and would not be causally linked. However, the receiver with the shorter latency would appear to excite the receiver with the longer latency. Moreover, if the unmeasured signal was roughly oscillatory (e.g., meandering back and forth on a time-scale comparable to the difference in latencies), then the receiver with the longer latency would appear to inhibit the receiver with the shorter latency.

In summary, while we believe that most causal interactions would result in a signal captured by our SDE model, the reverse is certainly not true. Causality can only truly be determined after following up our analysis with a controlled study wherein one of the variables is perturbed directly while measuring the response of the other variables.

Finally, we remark that, while dolphins and humans share many age-related qualities [18], they are also different in important ways. For example, female dolphins do not experience menopause, and thus would not be expected to exhibit the suite of hormonal changes that human women do as they age [74]. Further work is needed to determine which of the interactions we have discovered are truly causal, which affect (or are affected by) aging, and which generalize to humans.

5 Methods and Materials

5.1 Study Population and Animal Welfare

This study was limited to archived, retrospective health data and biospecimen analyses that were collected on Navy bottlenose dolphins (Tursiops truncatus) as part of their routine health care. The US Navy Marine Mammal Program is an Association for Assessment and Accreditation of Laboratory Animal Care International-certified program that adheres to animal care and welfare requirements outlined by the Department of Defense and US Navy Bureau of Medicine.

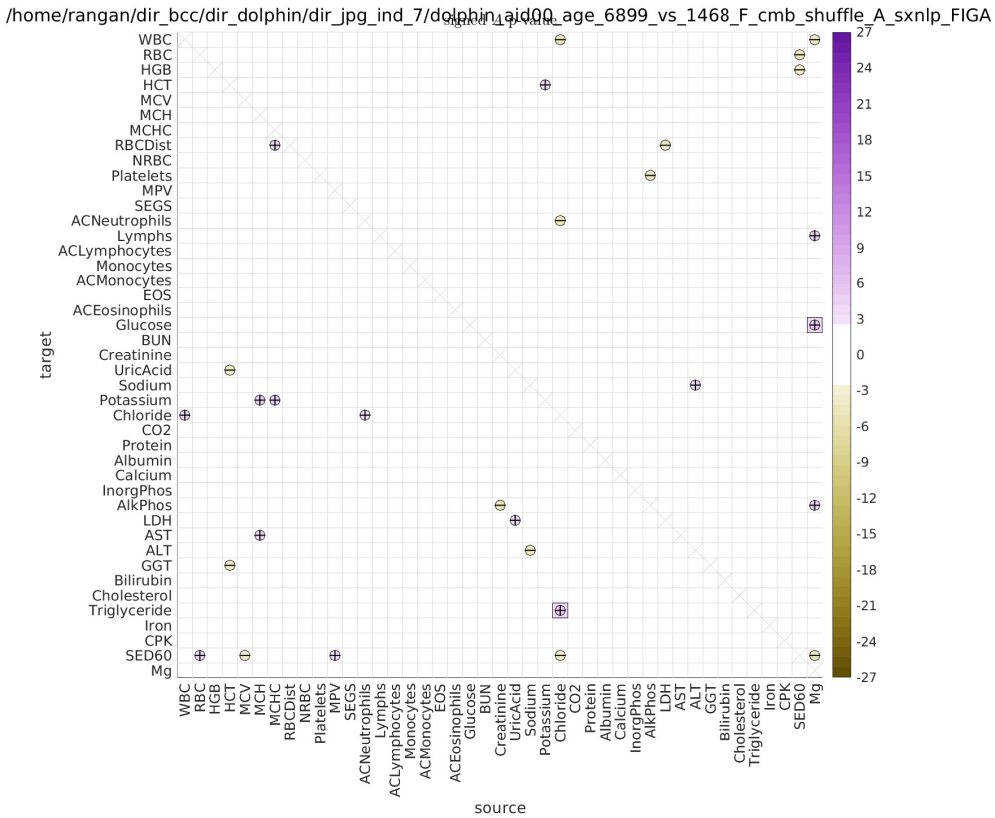

Figure 11: Here we illustrate significant differences in the deterministic interactions $A_{vv'}$ between (i) female dolphins over age 30 and (ii) female dolphins between the ages of 10 and 30.

5.2 Sample and Data Collection

Archived data for this study were limited to measures obtained from routine blood samples collected from Navy bottlenose dolphins in the morning following an overnight fast between January 1994 and December 2018 ($n = 5889$ samples from 144 dolphins). Blood samples collected either as an initial response or follow-up to acute clinical health concerns were excluded. Methods of routine blood sampling and the measurements obtained from the Navy dolphins have been described previously [18, 57, 35]. Data on the following 44 measures were available for analysis, of which we use $N = 43$: red blood cell indices (RBC count (RBC), hemoglobin (HGB), hematocrit (HCT), mean corpuscular volume (MCV), mean corpuscular hemoglobin (MCH), mean corpuscular hemoglobin concentration (MCHC), RBC distribution width (RBCDist, or RDW), and nucleated RBCs (NRBC)); platelets and mean platelet volume (MPV); white blood cell count (WBC); eosinophils (EOS), lymphocytes (Lymphs), monocytes, and neutrophils (SEGS) (percent and absolute counts, with the latter prefixed by 'AC'); glucose, blood urea nitrogen (BUN), creatinine, uric acid, sodium, potassium, chloride, carbon dioxide (CO2), total protein, albumin, calcium, inorganic phosphate (InorgPhos), alkaline phosphatase (AlkPhos), lactate dehydrogenase (LDH), aspartate aminotransferase (AST), alanine aminotransferase (ALT), gamma-glutamyl transpeptidase (GGT), bilirubin, total cholesterol, triglycerides, iron, creatine kinase (CPK), erythrocyte sedimentation rate (SED60), magnesium (Mg), and estimated glomerular filtration rate (GFR).

5.3 Relationships Between Biomarkers

Preprocessing: For two of the biomarkers we excluded measurements with atypical lab-codes that lay outside the standard range of measurements seen from the two most common lab-codes. This involved removing Albumin measurements below 2, and RBC distribution width (RDW) measurements above 40. We also ignored the glomerular filtration rate (GFR) variable, as for this data-set the GFR measurements v are functionally related to the Creatinine measurements v' (up to rounding/discretization error) as:

$$4\log^2(v') = 3\log^2\left(\frac{300}{v}\right). \tag{3}$$

Consequently, after applying the log-transformation described below, these two variables become (almost) exactly correlated with one another.

Log-transform: For each biomarker, we applied a log-transformation (adding the smallest discrete increment as a psuedocount) when such a transformation would reduce the skewness of the resulting distribution (across all dolphins). For this data-set the list of variables undergoing a log-transformation is: WBC, MCV, RDW, NRBC, ACNeutrophils, Lymphs, ACLymphocytes, Monocytes, EOS, ACEosinophils, Glucose, BUN, Creatinine, UricAcid, Potassium, Protein, Calcium, AlkPhos, LDH, AST, ALT, GGT, Bilirubin, Cholesterol, Triglyceride, Iron, CPK, SED60, GFR.

Normalization: For each dolphin we estimated the age-related drift for each biomarker by using linear-regression on measurements taken from age 5 onwards, excluding outliers above the 99th percentile or below the 1st percentile. We record the slope of this age-related linear drift for each biomarker for each dolphin, referring to this value later on to categorize individual dolphins as slow- or accelerated-agers (see Fig 14). After removing this linear drift term, we normalize each biomarker (for each dolphin) to have mean 0 and variance 1.

Analysis: For any particular subset of dolphins (e.g., male dolphins between the ages of 10 and 30), we fit a linear stochastic-differential-equation (SDE) to each pair of biomarkers, pooling observations across the dolphins in the chosen subset. Each of these SDEs has 12 parameters in total, accounting for type-A deterministic interactions, type-B shared stochastic drive, and type-C observation noise (see (1) and (2)). We performed the fit by first initializing $\boldsymbol{a}$ and A to be identically zero, and then iterating between (i) using linear-regression to estimate the entries of $BB^\intercal$ and $CC^\intercal$ while holding $\boldsymbol{a}$ and A fixed, and (ii) re-estimating $\boldsymbol{a}$ and A using a maximum-likelihood estimate with $BB^\intercal$ and $CC^\intercal$ fixed. Over the course of each iteration we use the values of $\boldsymbol{a}$ and A (at the current iteration) to re-impute any missing data in the observations via the simple maximum-likelihood estimate based on the SDE itself (i.e., assuming B and C are zero in (1) and (2). We iterate between (i) and (ii) until the model parameters $\boldsymbol{a}$, A, $BB^\intercal$ and $CC^\intercal$ have converged (which typically requires $2-3$ iterations).

Null Hypothesis: To estimate significance for any subset of dolphins across any age-interval for any pair of variables, we compare the estimated parameters of our SDE-model to the parameters obtained after randomly permuting the time-labels of the measurements. Each label-shuffled trial $k = 1, \ldots, K$ is associated with a permutation of the time-labels π_k which randomly interchanges time-labels within each dolphin (but not across dolphins) within the given age-interval. These label-shuffled trials corresponds to sampling from the null hypothesis that the true interaction coefficient $A_{vv'}$ for any pair of variables is 0, while still maintaining many of the correlations between variables. Note that the same set of permutations $\{\pi_1, \ldots, \pi_K\}$ is used for the label-shuffled trials $1, \ldots, K$ across all variable-pairs v, v'. Consequently, we can use the correlations between different parameters estimated from the same label-shuffled trial to adjust the p-values of any given parameter (see p_h below).

Uncorrected p-value: For each parameter we estimate the p-value 'p_0'numerically using $K = 256$ label-shuffled trials. When the parameter value for the original data is more extreme than the analogous parameter from any of the K label-shuffled trials, we estimate p_0 by first (i) estimating the z-score z_0 for that parameter using the gaussian-distribution fit to the collection of K label-shuffled parameter-values, and then (ii) estimating the p-value p_0 by applying a 2-sided test to the z-score z_0; i.e., $\log(p_0) = \mathrm{erfcln}(|z_0|/\sqrt{2})$.

Bonferroni Adjustment: To correct for multiple hypotheses we calculate two adjusted p-values 'p_b' and 'p_h'. The adjusted p-value p_b is obtained using a standard bonferroni-correction. Thus, $p_b = p_0/J$, where J is the number of parameters under consideration. For the deterministic interactions $A_{vv'}$ we set $J = N(N-1)$, while for the stochastic correlations $[BB^\intercal]_{vv'}$ we set $J = N(N-1)/2$ (recall $N = 43$ is the total number of variables analyzed).

Holm-Bonferroni Adjustment: Because the parameters observed for any label-shuffled trial are not uncorrelated with one another, this bonferroni-corrected p-value p_b is an overestimate (i.e., p_b is too conservative). A more accurate adjusted p-value 'p_h' can be obtained by using an empirical version of the holm-bonferroni adjustment. To describe this in detail consider the collection of $J = N(N-1)$ parameters $A_{vv'}$ for all variable-pairs $v \neq v'$. We first determine the J-element vector of these parameters for the original-data (by fitting each variable-pair individually). We'll refer to this vector of parameters as $\mathcal{A}_{:,0}$, with $\mathcal{A}_{j,0}$ referring to the jth parameter from the original data, and the colon ':' referring to 'all rows'. We then determine the corresponding vector for each of the K label-shuffled trials. We'll refer to each of these vectors as $\mathcal{A}_{:,k}$ for $k \in 1, \ldots, K$, one for each trial. Together, the $\mathcal{A}_{:,k}$ form a $J \times K$ array $\mathcal{A}_{:,:}$, with $\mathcal{A}_{j,k}$ referring to the jth parameter from trial k (the second colon on $\mathcal{A}_{:,:}$ refers to 'all columns'). To put these J different parameters on equal footing we first convert them all to z-scores; for each j we convert all the entries of $\mathcal{A}_{j,0}$ and $\mathcal{A}_{j,:}$ into z-scores using the gaussian-distribution fit to the collection of K entries in the row-vector $\mathcal{A}_{j,:}$. After converting each entry to a z-score, we apply a 2-sided test to convert each z-score to a negative-log-p-value $l = \mathrm{erfcln}(|z|/\sqrt{2})$. This procedure produces a vector of negative-log-p-values $\boldsymbol{l}_{j,0}$ corresponding to the original data, as well as an array $\boldsymbol{l}_{j,:}$ corresponding to the label-shuffled trials. Higher values of l indicate more significant values. Now we sort $\boldsymbol{l}_{:,0}$, as well as each of the $\boldsymbol{l}_{:,k}$ in the j-direction, in descending order. We'll refer to these j-sorted vectors as $\boldsymbol{l}'_{:,0}$ and $\boldsymbol{l}'_{:,k}$. For each rank-j (ranging from the largest and

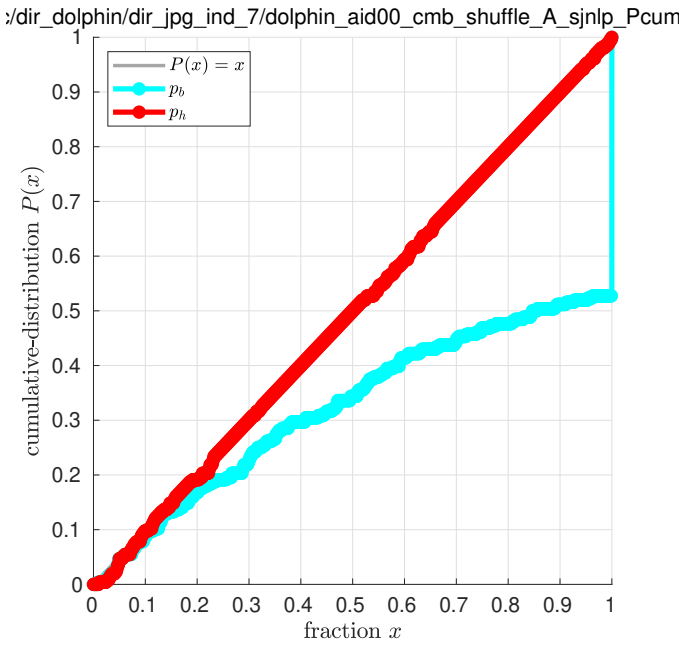

Figure 12: Here we illustrate (in red) the cumulative-distribution $P_h(x)$ for the holm-bonferroni adjustment, as calculated for the deterministic interaction terms $A_{vv'}$ across all variable-pairs for all dolphins and all ages. This cumulative-distribution $P_h(x)$ is defined to be the fraction of label-shuffled trials exhibiting at least one value of p_h (considered across all variable-pairs) less than x. An analogous cumulative-distribution $P_b(x)$ for the bonferroni-correction is shown in cyan. The value of $P_h(x)$ closely aligns with the identity line (grey).

most significant at rank-1 to the smallest and least significant at rank-J), we fit the K sorted negative-log-p-values $\boldsymbol{l}'_{j,:}$ with a gumbel-distribution, denoted by $G_j(l')$. We then use the distribution $G_j(\cdot)$ to ascribe a (one-sided) p-value p'_h to the value $\boldsymbol{l}'_{j,0}$. Finally, we set the adjusted p-value p_h to be $p_h = \max(p'_h, p_0)$. We can confirm that our holm-bonferroni adjusted p-value p_h is more accurate than the original bonferroni-adjusted p_b by measuring the fraction $P_h(x)$ of label-shuffled trials with at least one holm-bonferroni adjusted p-value (taken across the J variable-pairs) less than x. This cumulative-distribution function is quite close to the line $P_h(x) = x$, indicating that p_h is an accurate estimate of the true p-value, after adjusting for multiple hypotheses (see Fig 12).

Estimating Significant Differences: To search for significant differences between two different subsets of dolphins, we employ the same strategy described above, except applied to the difference between parameters (rather than the parameters themselves). Additionally, when comparing two different subsets we use all pairs of permutations π_k,$\pi_{k'}$ to define the label-shuffled distribution. To be more explicit, imagine that the first set is 'dolphins between the ages of 10 and 30', while the second set is 'dolphins over the age of 30'. We'll denote these two sets by S^1 and S^2. Continuing with the example we used above when discussing the holm-bonferroni adjustment, we would measure the J parameters $A_{vv'}$ (across all variable-pairs v, v') for each set, denoting the results with the vectors $\mathcal{A}^1_{:,0}$ and $\mathcal{A}^2_{:,0}$, respectively (note that here the superscript does not indicate an exponent, but rather the subset considered). We also do the same for each of the K label-shuffled trials, producing the arrays $\mathcal{A}^1_{:,:}$ and $\mathcal{A}^2_{:,:}$. Before proceeding any further we calculate the differences $\delta\mathcal{A}_{:,0} = \mathcal{A}^2_{:,0} - \mathcal{A}^1_{:,0}$ for the original data, and the K^2 differences $\delta\mathcal{A}_{:,k''} = \mathcal{A}^2_{:,k} - \mathcal{A}^1_{:,k'}$ for each pair of label-shuffled trials, where the index $k'' = 1, \ldots, K^2$ enumerates all the trial-pairs k, k'. From here on we proceed as usual, replacing (respectively) the vector $\mathcal{A}_{:,0}$ and the $J \times K$ array $\mathcal{A}_{:,:}$ with the vector $\delta\mathcal{A}_{:,0}$ and the $J \times K^2$ array $\delta\mathcal{A}_{:,:}$. An example of adjusted p-values produced using this approach is shown in Fig 13.

Estimating Aging-rate: To demonstrate consistency with the analysis of [35], we measure the slope of the age-related drift for the 6 biomarkers Hemoglobin (HGB), Alkaline Phosphatase, Platelets, Lymphocytes, Creatinine and Protein across each of the dolphins from age 10yr onwards. We project all dolphins onto the first principal-component 'u' of this array, separating them into two categories based on the median of u. Those dolphins with larger-than-median u-values typically exhibit slow deterioration of Hemoglobin, Alkaline Phosphatase, Platelets and Lymphocytes, along with a slow accumulation of Creatinine and Protein; these are classified as slow-agers. Conversely, the dolphins with lower-than-median u-values typically exhibit rapid deterioration of Hemoglobin, Alkaline Phosphatase, Platelets and Lymphocytes, along with rapid accumulation of Creatinine and Protein; these are classified as accelerated-agers. As shown in Fig 14, the accelerated-agers tend to develop anemia and lymphopenia and clinically low levels of alkaline phosphatase and platelets more rapidly than the slow-agers.

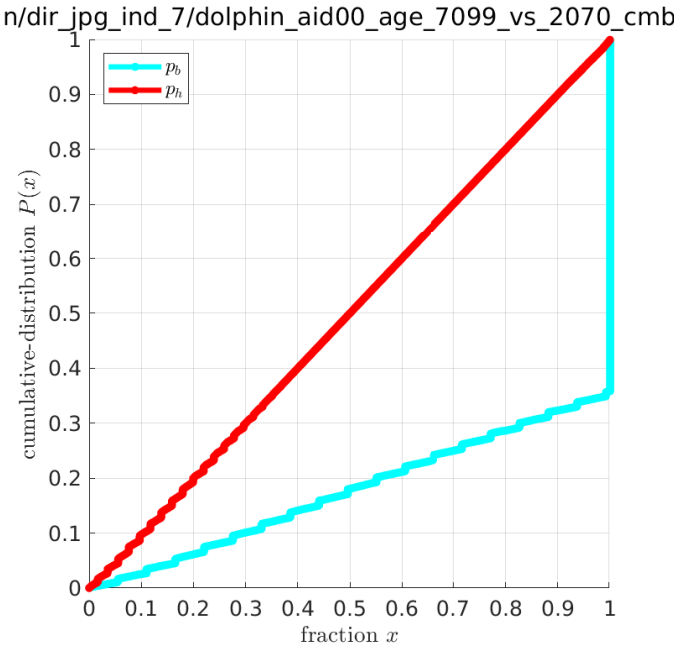

Figure 13: This figure has the same format as Fig 12. As before the cumulative-distribution is calculated for the deterministic interaction terms $A_{vv'}$ across all variable-pairs. However, this time the p-values refer to the significance of the difference (in parameters) between the subsets S^2 and S^1, where the former refers to dolphins over the age of 30, and the latter to dolphins between the ages of 10 and 30.

References

[1] T. Flatt and L. Partridge. Horizons in the evolution of aging. *BMC Biol.*, 16:93, 2018.

[2] Mark A. McCormick and Daniel E.L. Promislow. Recent advances in the systems biology of aging. *Antioxidants & Redox Signaling*, 29(10):973–984, 2018. PMID: 29020802.

[3] Morgan E. Levine. Modeling the Rate of Senescence: Can Estimated Biological Age Predict Mortality More Accurately Than Chronological Age? *The Journals of Gerontology: Series A*, 68(6):667–674, 12 2012.

[4] Jason L. Sanders, Ryan L. Minster, M. Michael Barmada, Amy M. Matteini, Robert M. Boudreau, Kaare Christensen, Richard Mayeux, Ingrid B. Borecki, Qunyuan Zhang, Thomas Perls, and Anne B. Newman. Heritability of and Mortality Prediction With a Longevity Phenotype: The Healthy Aging Index. *The Journals of Gerontology: Series A*, 69(4):479–485, 08 2013.

[5] J. Zierer, G. Kastenmüller, K. Suhre, C. Gieger, V. Codd, P. C. Tsai, J. Bell, A. Peters, K. Strauch, H. Schulz, S. Weidinger, R. P. Mohney, N. J. Samani, T. Spector, M. Mangino, and C. Menni. Metabolomics profiling reveals novel markers for leukocyte telomere length. *Aging*, 8:77–94, 2016.

[6] Daniel W. Belsky, Avshalom Caspi, Renate Houts, Harvey J. Cohen, David L. Corcoran, Andrea Danese, HonaLee Harrington, Salomon Israel, Morgan E. Levine, Jonathan D. Schaefer, Karen Sugden, Ben Williams, Anatoli I. Yashin, Richie Poulton, and Terrie E. Moffitt. Quantification of biological aging in young adults. *Proceedings of the National Academy of Sciences*, 112(30):E4104–E4110, 2015.

[7] A. B. Newman, N. W. Glynn, C. A. Taylor, P. Sebastiani, T. T. Perls, R. Mayeux, K. Christensen, J. M. Zmuda, S. Barral, J. H. Lee, E. M. Simonsick, J. D. Walston, A. I. Yashin, and E. Hadley. Health and function of participants in the long life family study: A comparison with other cohorts. *Aging*, 3:63–76, 2011.

[8] Joris Deelen, Johannes Kettunen, Krista Fischer, Ashley van der Spek, Stella Trompet, Gabi Kastenmüller, Andy Boyd, Jonas Zierer, Erik B. van den Akker, Mika Ala-Korpela, Najaf Amin, Ayse Demirkan, Mohsen Ghanbari, Diana van Heemst, M. Arfan Ikram, Jan Bert van Klinken, Simon P. Mooijaart, Annette Peters, Veikko Salomaa, Naveed Sattar, Tim D. Spector, Henning Tiemeier, Aswin Verhoeven, Melanie Waldenberger, Peter Würtz, George Davey Smith, Andres Metspalu, Markus Perola, Cristina Menni, Johanna M. Geleijnse, Fotios Drenos, Marian Beekman, J. Wouter Jukema, Cornelia M. van Duijn, and P. Eline Slagboom. A metabolic profile of all-cause mortality risk identified in an observational study of 44,168 individuals. *Nature Communications*, 10, 2019.

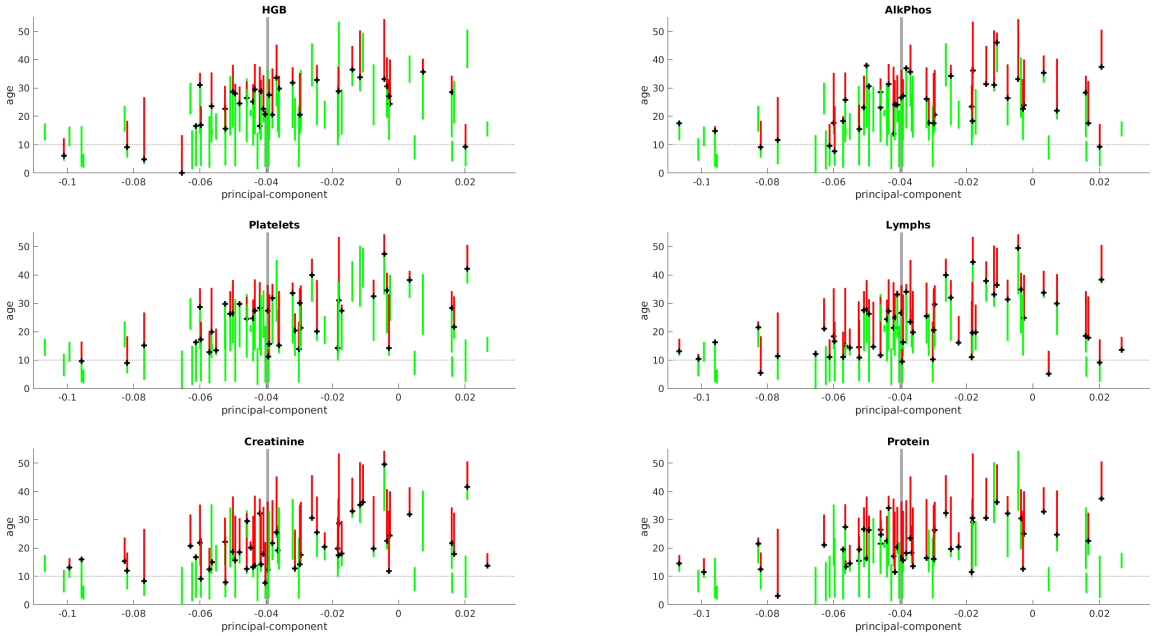

Figure 14: Here we illustrate the distribution of dolphins with regards to aging rate. As described in the Methods, we have measured the slope of the age-related drift for the 6 biomarkers HGB, AlkPhos, Platelets, Lymphocytes, Creatinine and Protein, using only measured ages above 10 years. We calculated the first principal-component u of this array, and projected each dolphin onto this principal-component. In each subplot we illustrate the correlation between age-related conditions and the u-value for each dolphin. Taking the first subplot (HGB) as an example, each dolphin is illustrated using a vertical line positioned at that dolphin's u-value. Each vertical line spans the dolphin's measured ages, with green segments indicating ages where the dolphin exhibits normal values of HGB, and red segments indicating ages after which the dolphin first exhibited a low value of HGB (i.e., anemia). The threshold we use to distinguish normal HGB from anemia is the value of HGB=12 listed in table-2 of [35]. For visual clarity we place a black '+' at the age when each dolphin first exhibits a low HGB value. One can clearly see a correlation between the u-value for each dolphin and the age at which that dolphin first exhibits anemia. The remaining subplots are analogous to the first, referencing the other 5 age-related variables described in table-2 of [35]. In the background of each subplot we highlight the median value of $u \sim -0.04$, which we use as a threshold to categorize dolphins into slow-agers ($u > -0.04$) and accelerated-agers ($u < -0.04$).

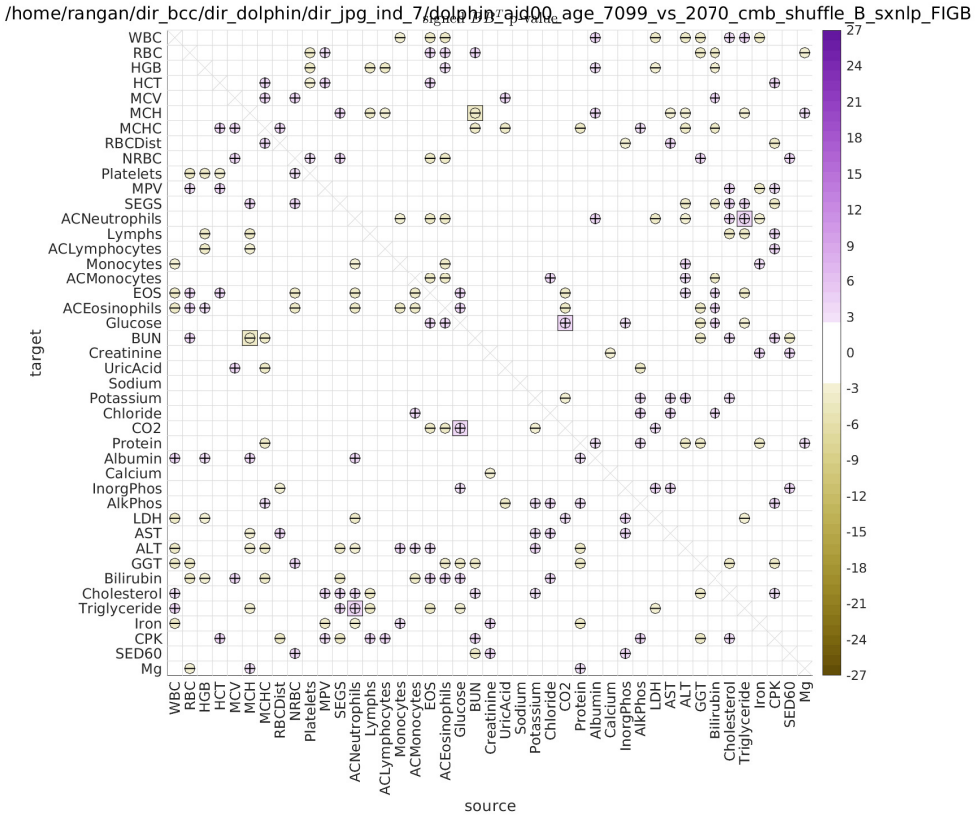

Figure 15: Supplementary Figure: This figure has the same format as Fig 9, showing the significant differences in the stochastic correlations $[BB^{\intercal}]_{vv'}$ between (i) dolphins over age 30 and (ii) dolphins between the ages of 10 and 30.

[9] Paola Sebastiani, Bharat Thyagarajan, Fangui Sun, Nicole Schupf, Anne B. Newman, Monty Montano, and Thomas T. Perls. Biomarker signatures of aging. *Aging Cell*, 16(2):329–338, 2017.

[10] Arti Hurria, Christopher R. Carpenter, Frances McFarland, Nancy E. Lundebjerg, Rafael de Cabo, Luigi Ferrucci, Stephanie A. Studenski, Nir Barzilai, Josephine P. Briggs, Joachim H. Ix, Dalane W. Kitzman, George A. Kuchel, Nicolas Musi, John C. Newman, Thomas A. Rando, Alexander K. Smith, Jeremy D. Walston, James L. Kirkland, and Raymond Yung. Models and studies of aging: Executive summary of a report from the u13 conference series. *Journal of the American Geriatrics Society*, 67(3):428–433, 2019.

[11] Alan A. Cohen. Aging across the tree of life: The importance of a comparative perspective for the use of animal models in aging. *Biochimica et Biophysica Acta (BBA) - Molecular Basis of Disease*, 1864(9, Part A):2680–2689, 2018. Model Systems of Aging.

[12] Jason N. Bruck. Decades-long social memory in bottlenose dolphins. *Proceedings of the Royal Society B: Biological Sciences*, 280(1768):20131726, 2013.

[13] Marino L. A comparison of encephalization between odontocete cetaceans and anthropoid primates. *Brain Behav Evol*, 51:230–238, 1998.

[14] Michael R. McGowen, Lawrence I. Grossman, and Derek E. Wildman. Dolphin genome provides evidence for adaptive evolution of nervous system genes and a molecular rate slowdown. *Proceedings of the Royal Society B: Biological Sciences*, 279(1743):3643–3651, 2012.

[15] Stephen H. Montgomery, Jonathan H. Geisler, Michael R. McGowen, Charlotte Fox, Lori Marino, and John Gatesy. The evolutionary history of cetacean brain and body size. *Evolution*, 67(11):3339–3353, 2013.

[16] P.E. Bielec, D.S. Gallagher, J.E. Womack, and D.L. Busbee. Homologies between human and dolphin chromosomes detected by heterologous chromosome painting.

[17] Stephen J. O'Brien, Marilyn Menotti-Raymond, William J. Murphy, William G. Nash, Johannes Wienberg, Roscoe Stanyon, Neal G. Copeland, Nancy A. Jenkins, James E. Womack, and Jennifer A. Marshall Graves. The promise of comparative genomics in mammals. *Science*, 286(5439):458–481, 1999.

[18] S. Venn-Watson, C.R. Smith, F. Gomez, and E.D. Jense. Physiology of aging among healthy, older bottlenose dolphins (tursiops truncatus): comparisons with aging humans. *J. Comp. Physiol. B.*, 181:667–80, 2011.

[19] Big brains and blood glucose: Common ground for diabetes mellitus in humans and healthy dolphins. *Comparative Medicine*, 57(4), 2007.

[20] Stephanie Venn-Watson. Dolphins and diabetes: Applying one health for breakthrough discoveries. *Frontiers in Endocrinology*, 5:227, 2014.

[21] Giovanni Di Guardo. Cetaceans, models for human disease? *Research in Veterinary Science*, 119:43–44, 2018.

[22] Stephanie Venn-Watson, Kevin Carlin, and Sam Ridgway. Dolphins as animal models for type 2 diabetes: Sustained, post-prandial hyperglycemia and hyperinsulinemia. *General and Comparative Endocrinology*, 170(1):193–199, 2011.

[23] James D. Craik, James D. Young, and Christoper I. Cheeseman. Glut-1 mediation of rapid glucose transport in dolphin (tursiops truncatus) red blood cells. *American Journal of Physiology-Regulatory, Integrative and Comparative Physiology*, 274(1):R112–R119, 1998. PMID: 9458906.

[24] Rebecca Rimbach, Ahmad Amireh, Austin Allen, Brian Hare, Emily Guarino, Chana Kaufman, Hannah Salomons, and Herman Pontzer. Total energy expenditure of bottlenose dolphins (Tursiops truncatus) of different ages. *Journal of Experimental Biology*, 224(15), 08 2021. jeb242218.

[25] Stephanie Venn-Watson, Cynthia Smith, Sacha Stevenson, Celeste Parry, Risa Daniels, Eric Jensen, Veronica Cendejas, Brian Balmer, Michael Janech, Bejamin Neely, and Randall Wells. Blood-based indicators of insulin resistance and metabolic syndrome in bottlenose dolphins (tursiops truncatus). *Frontiers in Endocrinology*, 4:136, 2013.

[26] Iron indices in bottlenose dolphins (tursiops truncatus). *Comparative Medicine*, 62(6), 2012.

[27] Stephanie Venn-Watson, Celeste Benham, Kevin Carlin, Damian DeRienzo, and Judy St. Leger. HEMOCHROMATOSIS AND FATTY LIVER DISEASE: BUILDING EVIDENCE FOR INSULIN RESISTANCE IN BOTTLENOSE DOLPHINS (TURSIOPS TRUNCATUS). *Journal of Zoo and Wildlife Medicine*, 43(3s), 2012.

[28] Zobair Younossi, Frank Tacke, Marco Arrese, Barjesh Chander Sharma, Ibrahim Mostafa, Elisabetta Bugianesi, Vincent Wai-Sun Wong, Yusuf Yilmaz, Jacob George, Jiangao Fan, and Miriam B. Vos. Global perspectives on nonalcoholic fatty liver disease and nonalcoholic steatohepatitis. *Hepatology*, 69(6):2672–2682, 2019.

[29] Danièlle Gunn-Moore, Oksana Kaidanovich-Beilin, María Carolina Gallego Iradi, Frank Gunn-Moore, and Simon Lovestone. Alzheimer's disease in humans and other animals: A consequence of postreproductive life span and longevity rather than aging. *Alzheimer's & Dementia*, 14(2):195–204, 2018.

[30] I. Stylianaki, A.T. Komnenou, D. Posantzis, K. Nikolau, and Papaioannou N. Alzheimer's disease-like pathological lesions in an aged bottlenose dolphin (tursiops truncatus). *Vet. Rec. Case. Rep.*, 7:e000700, 2019.

[31] Luigi Ferrucci, Marta Gonzalez-Freire, Elisa Fabbri, Eleanor Simonsick, Toshiko Tanaka, Zenobia Moore, Shabnam Salimi, Felipe Sierra, and Rafael de Cabo. Measuring biological aging in humans: A quest. *Aging Cell*, 19(2):e13080, 2020.

[32] Tina W Wey, Émy Roberge, Véronique Legault, Joseph W Kemnitz, Luigi Ferrucci, and Alan A Cohen. An Emergent Integrated Aging Process Conserved Across Primates. *The Journals of Gerontology: Series A*, 74(11):1689–1698, 05 2019.

[33] Megan K. Stolen and Jay Barlow. A model life table for bottlenose dolphins (tursiops truncatus) from the indian river lagoon system, florida, u.s.a. *Marine Mammal Science*, 19(4):630–649, 2003.

[34] S.K. Venn-Watson, E.D. Jensen, C.R. Smith, M. Xitco, and S.H. Ridgway. Evaluation of annual survival and mortality rates and longevity of bottlenose dolphins (tursiops truncatus) at the united states navy marine mammal program from 2004 through 2013. *Journal of the American Veterinary Medical Association*, 246:893–898, 2015.

[35] Stephanie Venn-Watson, Eric D. Jensen, and Nicholas J. Schork. A 25-y longitudinal dolphin cohort supports that long-lived individuals in same environment exhibit variation in aging rates. *Proceedings of the National Academy of Sciences*, 117(34):20950–20958, 2020.

[36] Steven H. Strogatz. *Nonlinear Dynamics and Chaos: With Applications to Physics, Biology, Chemistry and Engineering*. Westview Press, 2000.

[37] C. W. Gardiner. *Handbook of stochastic methods for physics, chemistry and the natural sciences*, volume 13 of *Springer Series in Synergetics*. Springer-Verlag, Berlin, third edition, 2004.

[38] Paolo Baldi. *Stochastic calculus. An introduction through theory and exercises*. Cham: Springer, 2017.

[39] Lloyd N. Trefethen and David Bau. *Numerical Linear Algebra*. SIAM, 1997.

[40] C.W.J. Granger. Investigating casual relations by econometric models and cross-spectral methods. *Econometrica*, 37:424–438, 1969.

[41] Steven L. Bressler and Anil K. Seth. Wiener–granger causality: A well established methodology. *NeuroImage*, 58(2):323–329, 2011.

[42] Michael Eichler. *Causal Inference in Time Series Analysis*, chapter 22, pages 327–354. John Wiley & Sons, Ltd, 2012.

[43] Abdulnasser Hatemi-J. Multivariate tests for autocorrelation in the stable and unstable var models. *Economic Modelling*, 21(4):661–683, 2004. 7th Conference on Econometric Modelling for Africa.

[44] G. F. von Tempelhoff, O. Schelkunov, A. Demirhan, P. Tsikouras, W. Rath, E. Velten, and R. Csorba. Correlation between blood rheological properties and red blood cell indices (mch, mcv, mchc) in healthy women. *Clinical hemorheology and microcirculation*, 62:45–54, 2016.

[45] J.P. Gligoroska, S. Gontarev, V. Maleska, L. Efremova, D.S. Stojmanova, and S. Manchevska. Red blood cell variables and correlations with body mass components in boys aged 10-17 years. *Turkish Journal of Pediatrics*, 62:53–60, 2020.

[46] D.E. Johnston. Special considerations in interpreting liver function tests. *American family physician*, 59:2223–2230, 1999.

[47] V. Lala, A. Goyal, P. Bansal, and D.A. Minter. Liver function tests. *StatPearls [Internet]. Treasure Island (FL): StatPearls Publishing;*, 2021.

[48] M. Straat, R. van Bruggen, D. de Korte, and N. P. Juffermans. Red blood cell clearance in inflammation. *Transfusion medicine and hemotherapy*, 39:353–361, 2012.

[49] E. Nemeth and T. Ganz. Anemia of inflammation. *Hematol Oncol Clin N Am*, 28:671–681, 2014.

[50] Frank A. D. T. G. Wagener, Eric Feldman, Theo de Witte, and Nader G. Abraham. Heme induces the expression of adhesion molecules icam-1, vcam-1, and e selectin in vascular endothelial cells. *Proceedings of the Society for Experimental Biology and Medicine*, 216(3):456–463, 1997.

[51] Frank A. D. T. G. Wagener, Andreas Eggert, Otto C. Boerman, Wim J. G. Oyen, Albert Verhofstad, Nader G. Abraham, Gosse Adema, Yvette van Kooyk, Theo de Witte, and Carl G. Figdor. Heme is a potent inducer of inflammation in mice and is counteracted by heme oxygenase. *Blood*, 98(6):1802–1811, 09 2001.

[52] Russell P. Rother, Leonard Bell, Peter Hillmen, and Mark T. Gladwin. The Clinical Sequelae of Intravascular Hemolysis and Extracellular Plasma HemoglobinA Novel Mechanism of Human Disease. *JAMA*, 293(13):1653–1662, 04 2005.

[53] Timothy H. Pohlman and John M. Harlan. Adaptive responses of the endothelium to stress. *Journal of Surgical Research*, 89(1):85–119, 2000.

[54] Aurelio V. Grac-a Souza, Maria Augusta B. Arruda, Marta S. de Freitas, Christina Barja-Fidalgo, and Pedro L. Oliveira. Neutrophil activation by heme: implications for inflammatory processes. *Blood*, 99(11):4160–4165, 06 2002.

[55] R. Mendonca, A.A.A. Silveira, and N. Conran. Red cell damps and inflammation. *Inflammation Research*, 65:665–678, 2016.

[56] E. Lang, S. Gatidis, N. F. Freise, H. Bock, R. Kubitz, C. Lauermann, H. M. Orth, C. Klindt, M. Schuier, V. Keitel, M. Reich, G. Liu, S. Schmidt, H. C. Xu, S. M. Qadri, D. Herebian, A. A. Pandyra, E. Mayatepek, E. Gulbins, F. Lang, and P. A. Lang. Conjugated bilirubin triggers anemia by inducing erythrocyte death. *Hepatology*, 61:275–284, 2015.

[57] S. Venn-Watson, E.D. Jensen, and S.H. Ridgway. Effects of age and sex on clinicopathologic reference ranges in a healthy managed atlantic bottlenose dolphin population. *Journal of the American Veterinary Medical Association*, 231:596–601, 2007.

[58] M.M. Eldibany, K.F. Totonchi, N.J. Joseph, and D. Rhone. Usefulness of certain red blood cell indices in diagnosing and differentiating thalassemia trait from iron-deficiency anemia. *American Journal of Clinical Pathology: Hematopathology*, 111:676–682, 1999.

[59] N. Li, H. Zhou, and Q. Tang. Red blood cell distribution width: A novel predictive indicator for cardiovascular and cerebrovascular diseases. *Disease Markers*, a:7089493, 2017.

[60] Kathy Doig and Bei Zhang. A methodical approach to interpreting the red blood cell parameters of the complete blood count. *American Society for Clinical Laboratory Science*, 30(3):173–185, 2017.

[61] B.S. Maner and L. Moosavi. Mean corpuscular volume. *StatPearls [Internet]. Treasure Island (FL): StatPearls Publishing*, 2021.

[62] Tove Skjelbakken, Jostein Lappegård, Trygve S. Ellingsen, Elizabeth Barrett-Connor, Jan Brox, Maja-Lisa Løchen, Inger Njølstad, Tom Wilsgaard, Ellisiv B. Mathiesen, Sigrid K. Brækkan, and John-Bjarne Hansen. Red cell distribution width is associated with incident myocardial infarction in a general population: The tromsø study. *Journal of the American Heart Association*, 3(4):e001109, 2014.

[63] Y. Hu, H. Liu, S. Fu, J. Wan, and X. Li. Red blood cell distribution width is an independent predictor of aki and mortality in patients in the coronary care unit. *Kidney Blood Press Res*, 42:1193–1204, 2017.

[64] Alan E. Dugdale and Tony Badrick. Red blood cell distribution width (rdw)—a mechanism for normal variation and changes in pathological states. *Journal of Laboratory and Precision Medicine*, 3(0), 2018.

[65] Luke C. Pilling, Janice L. Atkins, Michael O. Duff, Robin N. Beaumont, Samuel E. Jones, Jessica Tyrrell, Chia-Ling Kuo, Katherine S. Ruth, Marcus A. Tuke, Hanieh Yaghootkar, Andrew R. Wood, Anna Murray, Michael N. Weedon, Lorna W. Harries, George A. Kuchel, Luigi Ferrucci, Timothy M. Frayling, and David Melzer. Red blood cell distribution width: Genetic evidence for aging pathways in 116,666 volunteers. *PLOS ONE*, 12(9):1–14, 09 2017.

[66] Z. Yan, Y. Fan, Z. Meng, C. Huang, M. Liu, Q. Zhang, K. Song, and Q. Jia. The relationship between red blood cell distribution width and metabolic syndrome in elderly chinese: a cross-sectional study. *Lipids in Health and Disease*, 18, 2019.

[67] Adela Hruby, James B. Meigs, Christopher J. O'Donnell, Paul F. Jacques, and Nicola M. McKeown. Higher magnesium intake reduces risk of impaired glucose and insulin metabolism and progression from prediabetes to diabetes in middle-aged americans. *Diabetes Care*, 37(2):419–427, 2014.

[68] N. Veronese, S. Watutantrige-Fernando, C. Luchini, M. Solmi, G. Sartore, G. Sergi, E. Manzato, M. Barbagallo, S. Maggi, and B. Stubbs. Effect of magnesium supplementation on glucose metabolism in people with or at risk of diabetes: a systematic review and meta-analysis of double-blind randomized controlled trials. *European Journal of Clinical Nutrition*, 70:1354–1359, 2016.

[69] Fouad R. Kandeel, Emilia Balon, Stephen Scott, and Jerry L. Nadler. Magnesium deficiency and glucose metabolism in rat adipocytes. *Metabolism*, 45(7):838–843, 1996.

[70] G. Paolisso, A. Scheen, F. D'Onofrio, and P. Lefebvre. Magnesium and glucose homeostasis. *Diabetologia*, 33:511–4, 1990.

[71] W. H. Linda Kao, Aaron R. Folsom, F. Javier Nieto, Jing-Ping Mo, Robert L. Watson, and Frederick L. Brancati. Serum and Dietary Magnesium and the Risk for Type 2 Diabetes Mellitus: The Atherosclerosis Risk in Communities Study. *Archives of Internal Medicine*, 159(18):2151–2159, 10 1999.

[72] M. Barbagallo, M. Belvedere, and L.J. Dominguez. Magnesium homeostasis and aging. *Magnesium Research*, 22:235–46, 2009.

[73] G. Paolisso, S. Sgambato, A. Gambardella, G. Pizza, P. Tesauro, M. Varricchio, and F. D'Onofrio. Daily magnesium supplements improve glucose handling in elderly subjects. *Am J Clin Nutr*, 55:1161–7, 1992.

[74] Caitlin Karniski, Ewa Krzyszczyk, and Janet Mann. Senescence impacts reproduction and maternal investment in bottlenose dolphins. *Proceedings of the Royal Society B: Biological Sciences*, 285(1883):20181123, 2018.